全球地震波伝播シミュレーション

課題責任者
坪井　誠司　　　海洋研究開発機構 付加価値情報創生部門 地球情報基盤センター

著者
坪井　誠司*1， Rhett Butler*2
*1 海洋研究開発機構 付加価値情報創生部門 地球情報基盤センター， *2 University of Hawai'i

本報告では、地球内核内の深さ約 100km 付近での速い S 波速度を示す明らかな不連続面についての地震学的証拠を示す。内核を横断する 5 つの地震—観測点経路に対して対蹠点（> 179°）のデータをスタックした。 アルジェリアのタマンラセット（TAM）とトンガの地震、およびブラジルのピティンガ（PTGA）とスラウェシの地震の間の経路では、PKIIKP（内核境界での下側反射）の明確な先駆波がみられる。スタックした波形（T> 4 秒）を、地球シミュレータによりモデル化し、16 個を超える内核地震波構造モデルを試した。その結果、内核境界の下 100km の深さで液体/固体界面の下で反射するものとしてうまくモデル化出来ることが分かった。この境界は反射率が高く、5km/s 以上のせん断波速度コントラストに敏感である。さらに TAM と PTGA で観察される後続波は、内核表面下深さ約 250km 付近の明らかな不連続性としてモデル化できる可能性がある。

キーワード：数値波形計算、地震波動、地球内核

1.はじめに

地震の対蹠点で得られる地震波は、地球中心核の構造に独自の制約を提供する。Δ= 180°の地震の対蹠点に伝播する際、対蹠点の近くでは波が集束し、地震エネルギーが増幅される[1–8]。対蹠点への地震波伝播を構成する波線の表面は、震源と対蹠点との間の直径の周りで地球を囲んでいる。 PKIKP 波のみがこの直径に沿って伝播し、対蹠点では増幅されないが、固有の直径で指定された対蹠点を直径方向に確認することに用いることができる。波線経路が内核境界（ICB）の波長サイズの「パッチ」をサンプリングする可能性がある対蹠点よりも短い距離では、PKIIKP は、その直径に直交する ICB を含む大円領域をサンプリングする。さらに、ICB の 50 km の PKIIKP 波長の場合、PKIIKP は対蹠点を通らない波よりも約 2 桁多い ICB の領域をサンプリングすることが分かる。

2 データセット

トンガからアルジェリア、スラウェシからアマゾン、チリ北部から海南島、そしてチリ中部と中国本土の間の 2 つの直径からの地震データを調べた。 TAM、PTGA、QIZ、ENH、XAN の各観測点の対蹠点で利用可能な地震データを収集した。各対蹠観測点の選択された波形を図 1 に示す。 TAM と PTGA の波形データは、PKIKP と PKIIKP の間に有意な到着があることを示しており、 PKIIKP の約 7 秒と約 17 秒前に到着している。中国の観測点（QIZ、ENH、XAN）に対し、TAM と PTGA は対照的であり、ENH、XAN、および QIZ ではこの波形の到達は見られない。 5 つの直径の波の伝播経路が地殻、マントル、または外核の共通の経路を共有していないことを考慮して、信号対雑音比を改善するために 5 つの直径のそれぞれにスタッキングを行った。これらの方法には、振幅および位相加重スタッキング[9]に加えて波線パラメータに沿ったスラントスタッキング[3]が含まれる。図 1 の振幅と位相加重スタックは、PKIKP と PKIIKP の間の地震波の到着が大きく（TAM と PTGA）、これらが小さい（XAN、ENH、および QIZ）観測点間の大まかな境界を示している。これらの結果は、明確な PKIIKP 前駆波を持つ TAM と

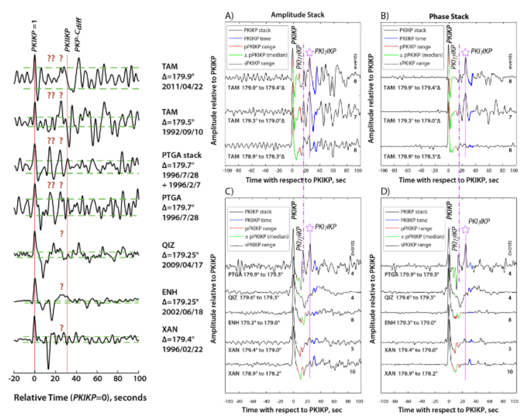

図 1.（左）分析と波形モデリングのために選択された対蹠点データ。観測点、距離、地震の発生日を示す。（右）対蹠点データの振幅（A および C）スタックと位相（B および D）スタックがプロットされ、距離範囲とイベント数を示す。 波形とスタックデータは PKIKP に正規化され、PKIIKP の PREM による走時時間が示されている。 TAM と PTGA のデータは、PKIKP と PKIIKP の間の複雑な到着（「？」と「??」のラベル）を示している（暫定的に PKI？IKP と PKI ?? IKP のラベルが付けられ、TAM と PTGA の間で整列（紫）されている）。

PTGA、および前駆波が見えない QIZ、ENH、XAN の二つのグループを示している。 PKIKP と

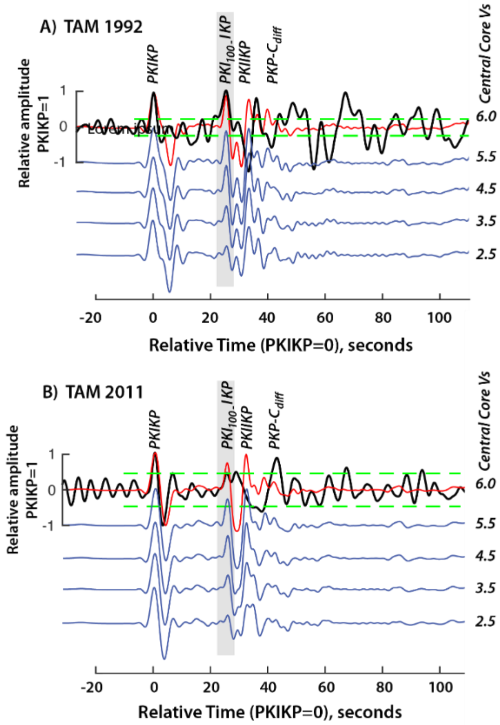

図 2. .PKI100-IKP の振幅は、深さ 100km で S 波速度を 2.5 から 5.5 km / s まで増加させた 3DSEM（青）の深増加している。 赤は 6.0 km / s の場合である。。データは黒でプロットされ、±2σイベント前のノイズは緑で示されている。 振幅と時間は PKIKP に正規化されている。

PKIIKP の間のエネルギーは、PKIIKP よりも内側のコアを介して深く早く伝播すると仮定して、前駆波は、内側のコアでの不確実な起源を反映して、暫定的に PKI?IKP および PKI ?? IKP と呼ぶ。

3.シミュレーション：3D スペクトル要素モデリング

対蹠点データセットのモデリングでは、以前[4,7,8]のように 3D スペクトル要素法（3DSEM）[10–13]を使用した。使用したモデルには、コア用の単純な PREM モデル、地球マントル用の 3D トモグラフィモデル（s362wmani）[14]、地殻モデル CRUST2.0 [15]、および楕円率が組み込まれている。対蹠点観測のシミュレーションでは、グローバル CMT メカニズムと震源[16]を使用した。 3D マントルと地殻を組み込むことで、コアの上の構造（たとえば、上部マントル、D " およびコアとマントルの境界）から散乱されたエネルギーが 3DSEM シミュレーションに含まれる。 3DSEM の精度は T> 3.5 秒のため、データと 3DSEM に同じフィルターを使用して直接比較できるようにした。

上部内核の波形研究では、0.1～3 Hz [17]および～1 Hz [18～20]の伝搬帯域で深さ 100km 付近の P 波の不連続性の証拠はほとんど示されていない。 Cormier と Attanayake [21]は、約 0.5 Hz で、大西洋の下を中心とする ICB の 140 km 下で 1%の Vp の不連続性を発見したが、他の場所では明らかではない。最初に Vp のモデルを変更して PKIIKP 前駆波が再現できるか検討した。ここでは、モデルは内核の地震波速度は等方性を仮定した。深さ約 100km に固液境界を持つ一連のモデルは、PKI？IKP のタイミングを満たしたが、振幅は満たすことが出来なかった。内核 S 波構造の詳細は未解決であるが、3D 構造や異方性などの複雑さは、以前の P 波研究で明確に表現されている[22–24]。次に、Vs が PKI？IKP に与える影響を検討した。固液界面より下の Vs の値を変更すると、PKIKP および PKIIKP に対する到着時間を変更せずに、PKI？IKP の振幅を変更できた。

3.1.1TAM および PTGA

図 2 では、TAM の対蹠点にある 2011 年の正断層地震と 1992 年の逆断層地震の 2 つの地震をモデル化した。これらのモデルでは、Vp と密度は内核の PREM 値から変化させず、Vs は 2.5～2 のステップで変更させた。PKI？IKP / PKIKP で観測された相対振幅を達成するには、VS が 5 km / s 以上である必要があることが分かった。適切な振幅と到着時間を持つ候補位相があるため、PKI？IKP には、z = 100 km の深さの境界面からの下面反射として、PKI100 IKP という標準的な地震位相名をつけた。PKI100 IKP の PTGA スタック観測（図 2B）は、スタック振幅と位相加重比（PKIKP の> 50%）、および相対タイミングの両方で TAM に最も類似している。 PTGA スタックデータは、TAM の観測結果を裏付けている（図 2）。 TAM と PTGA は、共通の震源近傍、観測点近傍、マントル、および外核伝搬経路を共有しないため、TAM スタックと PTGA スタックに見られる共通点は、共有された内核構造にあると考えられる。ただし、この共有構造は、内核の 2 つの実質的に異なる部分に存在する必要がある。結果からは、PTGA が PREM にうまく適合していないことを示しており、到着時を考慮すると、PREM 構造の上にある深さ 250 km（150 km の厚さ、VS≥5km/ s）付近に明らかな不連続性を導入すると、PTGA データに適切に適合する。考慮した 2 つの端成分モデルは z = 100 km より上でのみ異なる（液体と固体）。PKI250-IKP はほぼ同じように表現され、たとえば、250km を超える構造は PKI250IKP に実質的に寄与していない。

ただし、P 波長が約 50 km の場合、100km または 250km の深さであるかどうかにかかわらず、鋭い境界面と狭い遷移勾配を簡単に区別できないことに注意しなければならない。これらのモデルは一意ではないが、データの本質を捉えている。

3.1.2 QIZ、ENH、および XAN

中国の QIZ、ENH、XAN、およびブラジルの PTGA の対蹠点スタックは、南アメリカと東南アジアの間のパスに対する PKI100-IKP の観測の実質的な多様性を示している（図 1）。 PTGA スタック結果は、QIZ、ENH、

および XAN のスタックとは大幅に異なっており中国の観測点データのスタックデータに PKI100-IKP が到着したという確固たる証拠はない。隣接する中国の観測点（QIZ、ENH、XAN）は、TAM および PTGA とは著しく対照的に、PREM モデルによりよく適合することを示している。

4.結果と分析

対蹠点で観測された PKIIKP 波の前駆波は、本研究の結果、内核境界の下 100km の深さで液体/固体界面の下で反射するものとしてうまくモデル化出来ることが分かった。この境界は反射率が高く、5km/s 以上のせん断波速度コントラストに敏感である。さらに TAM と PTGA で観察される後続波は、内核表面下深さ約 250km 付近の明らかな不連続性としてモデル化できる可能性がある。ここで新たに導入する PKI100 IKP 境界は、どこでも同じではなく、TAM と ENH の両方を同時に一致させるには、3 次元の最上部の内核構造を考慮する必要がある。 TAM-トンガ環は、チリと中国の観測所の間の環にほぼ直交していることは興味深い。

[1] Rial, J.A. and Cormier, V.F., 1980. Seismic waves at the epicenter's antipode. *Journal of Geophysical Research: Solid Earth*, *85*(B5), pp.2661-2668.

[2] Butler, R., 1986. Amplitudes at the antipode. *Bull. Seismol. Soc. Am.* 76, 1355–1365.

[3] Niu, F., and Chen, QF, 2008. Seismic evidence for distinct anisotropy in the innermost inner core. Nature Geosci., 1, 692–696 (2008). https://doi.org/10.1038/ngeo314

[4] Butler, R., and Tsuboi, S., 2010. Antipodal seismic observations of temporal and global variation at Earth's inner-outer core boundary. *Geophys. Res. Lett.* 37, L11301. https://doi.org/10.1029/2010GL042908https://doi.org/10.1029/2010GL042908.

[5] Cormier, V.F., 2015. Detection of inner core solidification from observations of antipodal PKIIKP. *Geophysical Research Letters*, *42*(18), pp.7459-7466.

[6] Attanayake, J., Thomas, C., Cormier, V. F., Miller, M. S., & Koper, K. D. (2018). Irregular transition layer beneath the Earth's inner core boundary from observations of antipodal PKIKP and PKIIKP waves. *Geochemistry, Geophysics, Geosystems, 19*. https://doi.org/10.1029/ 2018GC007562

[7] Tsuboi, S. and R. Butler, 2020. Inner core differential rotation rate inferred from antipodal seismic observations. P*hysics of Earth and Planetary Interiors*, 301, April 2020, 106451, doi.org/10.1016/j.pepi.2020.106451.

[8] Butler, R. and Tsuboi, S., 2020. Antipodal observations of global differential times of diffracted P and PKPAB within the D″ layer above Earth's core–mantle boundary. Geophysical Journal International, 222(1), pp.327-337.

[9] Schimmel, M. and Paulssen, H., 1997. Noise reduction and detection of weak, coherent signals through phase-weighted stacks. *Geophysical Journal International*, *130*(2), pp.497-505

[10] Komatitsch, D. & Vilotte, J.P., 1998, The spectral-element method: an efficient tool to simulate the seismic response of 2D and 3D geological structures, *Bull. seism. Soc. Am.*, **88,** 368–392.

[11] Komatitsch, D., Ritsema, J. & Tromp, J., 2002. The spectral-element method, Beowulf computing, and global seismology, *Science,* **298,** 1737–1742 (2002).

[12] Tsuboi, S., D. Komatitsch, C. Ji, and J. Tromp, 2003. Broadband modeling of the 2002 Denali Fault earthquake on the Earth Simulator. *Phys. Earth Planet. Inter.* 139, 305–312.

[13] Komatitsch, D., Tsuboi, S. & Tromp, J., 2005. The spectral-element in seis- mology, in *Seismic Earth: Array analysis of broadband seismograms*,eds Levander, A. & Nolet, G., *AGU Geophysical Monograph* 157, 2005, AGU, pp. 205–227.

[14] Kustowski, B., Ekström, G. and Dziewoński, A.M., 2008. Anisotropic shear-wave velocity structure of the Earth's mantle: A global model. *Journal of Geophysical Research: Solid Earth*, *113*(B6).

[15] Bassin, C., G. Laske, and G. Masters, 2000. The current limits of resolution for surface wave tomography in North America, Eos Trans. AGU, 81, F897.

[16] Ekström, G., M. Nettles, and A. M. Dziewonski, 2012. The global CMT project 2004-2010: Centroid-moment tensors for 13,017 earthquakes, Phys. Earth Planet. Inter., 200-201, 1-9doi:10.1016/j.pepi.2012.04.002.

[17] Stroujkova, A., and V. F. Cormier, 2004. Regional variations in the upper-most 100 km of the Earth's inner core, J. Geophys. Res., 109, B10307, doi:10.1029/2004JB002976

[18] Leyton, F., Koper, K.D., Zhu, L. and Dombrovskaya, M., 2005. On the lack of seismic discontinuities within the inner core. *Geophysical Journal International*, *162*(3), pp.779-786.

[19] Yu, W.C. and Wen, L., 2006. Seismic velocity and attenuation structures in the top 400 km of the Earth's inner core along equatorial paths. *Journal of Geophysical Research: Solid Earth*, *111*(B7).

[20] Cormier, V.F., Attanayake, J. and He, K., 2011. Inner core freezing and melting: Constraints from seismic body waves. *Physics of the Earth and Planetary Interiors*, *188*(3-4), pp.163-172.

[21] Cormier, V.F. and Stroujkova, A., 2005. Waveform search for the innermost inner core. *Earth and Planetary Science Letters*, 236(1-2), pp.96-105.

[22] Tanaka, S. and Hamaguchi, H., 1997. Degree one heterogeneity and hemispherical variation of anisotropy in the inner core from PKP (BC)–PKP (DF) times. *Journal of Geophysical Research: Solid Earth*, *102*(B2), pp.2925-2938.

[23] Ishii, M., and A. M. Dziewonski, 2002. The innermost inner core of the Earth: Evidence for a change in anisotropic behavior at the radius of about 300 km, *Proc. Natl. Acad. Sci. U. S. A.*, **99**, 14,026–14,030, doi:10.1073/pnas.172508499.

[24] Waszek, L. and Deuss, A., 2011. Distinct layering in the hemispherical seismic velocity structure of Earth's upper inner core. Journal of Geophysical Research: Solid Earth, 116(B12).

Antipodal Seismic Reflections upon Shear Wave Velocity Structures within Earth's Inner Core

Project Representative
Seiji Tsuboi Center for Earth Information Science and Technology, Research Institute for Value- Added-Information Generation, Japan Agency for Marine-Earth Science and Technology

Authors
Seiji Tsuboi[*1], Rhett Butler[*2]

[*1]Center for Earth Information Science and Technology, Research Institute for Value-Added- Information Generation, Japan Agency for Marine-Earth Science and Technology, [*2]University of Hawai‘i

Seismic evidence is presented for a high shear wave velocity, an apparent discontinuity near ~100 km depth within Earth's solid inner core. Antipodally (>179°) focused data are stacked for five source–receiver diametric ray paths traversing the inner core. Two antipodal paths follow ray surfaces which are aligned with diameters between Tamanrasset (TAM), Algeria and Tonga earthquakes and Pitinga (PTGA), Brazil and Sulawesi earthquakes, providing clear examples of precursors to *PKIIKP* (an underside reflection at the inner core boundary). Waveform and stacked data (T>4 seconds) were modeled via the Earth Simulator—testing more than 16 inner core model series with varying compressional and shear wave velocities in upper inner core structures. The precursory seismic phases are successfully modelled as reflecting beneath a core liquid/solid interface at 100 km depth below the inner core boundary. This interface is highly reflective, and sensitive to a shear wave velocity contrast ≥ 5 km/s. An earlier precursory phase is observed at TAM and PTGA which may be modeled as an apparent discontinuity near ~250 km depth.

Keywords: Antipodal seismic observation, Inner core structure, Spectral-element Method

1. Introduction

Complementing the body wave and normal mode research on Earth's core structure and properties, antipodal studies provide unique constraints. In propagating through the core to the earthquake's antipode at $\Delta = 180°$, the focusing of waves near the antipode amplifies seismic energy [1–8]. Near the antipode (>179°) of an earthquake, the seismic energy from all azimuths about the earthquake source coalesces together, and the individual ray paths merge into a ray surface. The ray surfaces comprising the antipodal propagation circumscribe the Earth about the diameter between earthquake source and receiving antipodal station. Although only *PKIKP* propagates along this diameter (Figure 1) and is not antipodally amplified, we find it convenient to review and discuss antipodal data diametrically as designated by their unique *diameters*. At distances less than antipodal where ray paths (e.g., *PKIIKP*, Figure 1) may sample a wavelength-size "patch" on the inner core boundary (ICB), the antipodal phase *PKIIKP* samples a great circle region encompassing the ICB orthogonal to that diameter. Furthermore, for a *PKIIKP* wavelength of 50 km on the ICB the antipodal phase samples about two orders of magnitude more of the ICB than the non-antipodal wave.

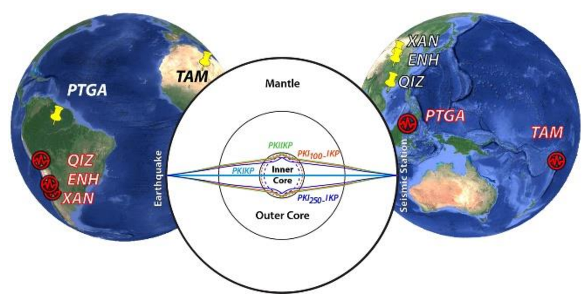

Figure 1. Maps show the locations of earthquakes (red symbols) and corresponding antipodal stations (red outlined). Locations of the antipodal seismic stations are labeled (yellow pins). Inset figure shows the antipodal ray paths for *PKIKP* (cyan), *PKIIKP* (green) and the suggested paths for the central core phases, $PKI_{100}\text{-}IKP$ (red) and $PKI_{250}\text{-}IKP$ (blue) . Path segments propagating in the Mantle, Outer Core, and Inner Core, are designated P, K, and I, respectively. Whereas *PKIIKP* (green) reflects beneath the ICB, $PKI_{100}\text{-}IKP$ (red) reflects beneath an interface in the upper inner core, demarcated by dotted red circle at 100 km depth. Similar, $PKI_{250}\text{-}IKP$ (blue) reflects beneath an interface in the upper inner core, demarcated by dotted blue circle at 250 km depth. Although ray paths are shown in this cross-section, the antipodal energy converges from all azimuths as a ray surface. The abridged names for $PKI_{100}\text{-}IKP$ and $PKI_{250}\text{-}IKP$ in the text are $PKI_{?}IKP$ and $PKI_{??}IKP$, respectively.

2 Data set

Seismic data from five diameters are examined (Figure 1)—Tonga to Algeria, Sulawesi to Amazon, northern Chile to

Hainan Island, and two between central Chile and the mainland China. We collected available earthquake data antipodal to the stations TAM, PTGA, QIZ, ENH, and XAN. Selected waveforms for each antipodal station are plotted in Figure 2, which are used in synthetically modeling features highlighted from stacking the antipodal data (Figure 2). The

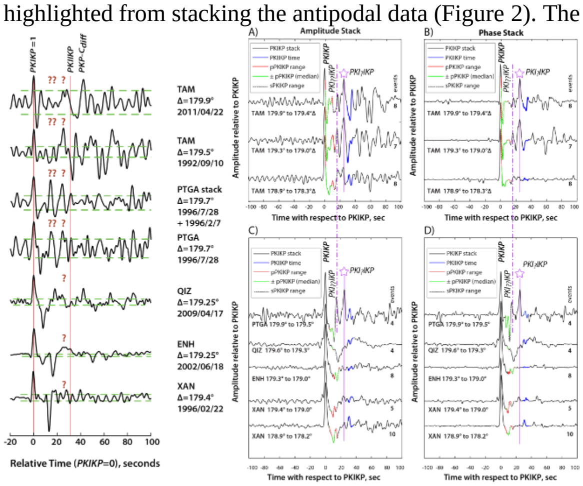

Figure 2. (left) Antipodal data selected for analysis and waveform modeling, noting the station, distance, and earthquake origin date. (right) Amplitude (AC) and phase (BD) stacks of antipodal data are plotted, noting distance range and numbers of events. The waveform and stacked data are normalized to PKIKP and the PREM travel time for PKIIKP is indicated. The heterogeneity of the data traversing the inner core is significant. The data for TAM and PTGA show complex arrivals (labeled "?" and "??") between PKIKP and PKIIKP—tentatively labeled PKI?IKP and PKI??IKP and aligned (violet) between TAM and PTGA—whereas for QIZ, ENH, and XAN the near-source surface reflection pPKIKP dominates.

waveform data for TAM and PTGA show significant arrivals between *PKIKP* and *PKIIKP*. arriving ~7 and ~17 seconds before *PKIIKP*. For the Chinese stations—QIZ, ENH, and XAN—the dichotomy with TAM and PTGA is striking. For ENH, XAN, and QIZ the evidence is subdued. Given that wave propagation paths for the five diameters do not share common paths in the crust, mantle, or outer core, we employed data stacking for each of the five diameters to improve their signal-to-noise ratios. These methods include amplitude and phase-weighted stacking [9] plus slant-stacking along ray parameter [3]. The amplitude and phase-weighted stacks in Figure 2 show a rough demarcation between stations where seismic arrivals between *PKIKP* and *PKIIKP* are large (TAM and PTGA) and small/negligible (XAN, ENH, and QIZ) excepting only the near-source, depth phase *pPKIKP*. The stacked data authenticate findings of the waveform data in Figure 2, that there are two distinct groups—TAM and PTGA with clear *PKIIKP* precursors and QIZ, ENH, and XAN where evidence is subdued. Hypothesizing that the energy between *PKIKP* and *PKIIKP* propagates deeper and earlier through the inner core than *PKIIKP* (which is a maximum time phase), the precursor phases are tentatively designated *PKI?IKP* and *PKI??IKP*, reflecting their uncertain origin in the inner core. Figure 2 clearly shows these parallel (in time) arrivals observed at TAM and PTGA.

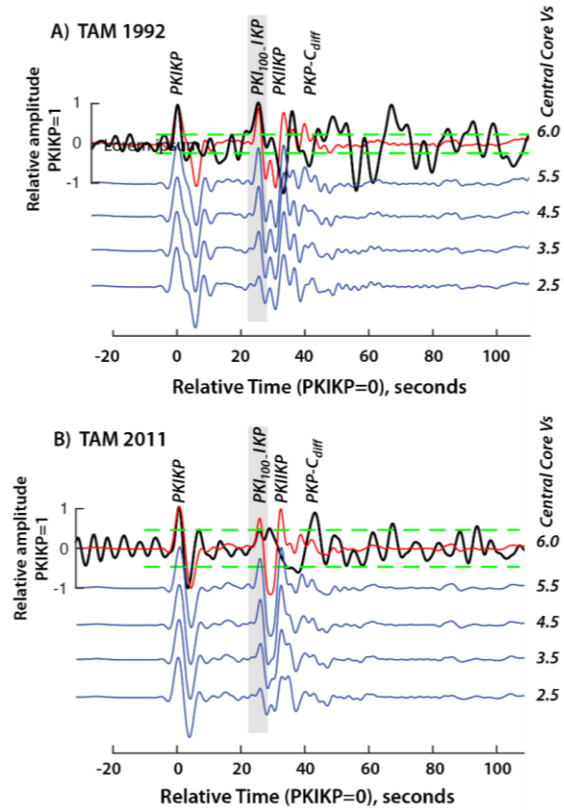

Figure 3. Amplitude of the inner core phase PKI100-IKP grows as VS increases below an apparent solid-liquid discontinuity at 100 km depth for synthetic TAM seismograms (blue), generated with successive shear wave velocities from 2.5 to 5.5 km/s, and (red) for 6.0 km/s. The relative timing of the core phase PKI100-IKP is indicated and shaded in gray, as observed near the antipode of TAM from earthquakes in 1992 and 2011. Data are plotted in black, with $\pm 2\sigma$ pre-event noise shown in green. Amplitudes and times are normalized to PKIKP.

3. Simulations: 3D Spectral Element Modeling

In modeling the antipodal data set, we approached the problem synthetically using the 3D spectral element method (3DSEM) [10–13] as previously applied [4,7,8]. The initial model used incorporates a simple PREM mode for the Core, a 3D tomographic model—*s362wmani*—for Earth's Mantle [14], crustal model CRUST2.0 [15], and ellipticity. In synthesizing the antipodal observations, global CMT mechanisms and locations [16] are used in modeling the earthquake sources. Incorporating a 3D mantle and crust, we include within the 3DSEM synthetics the energy scattered from structure above the core (e.g., upper mantle, D" and the core–mantle boundary). Since the 3DSEM synthetics are correct for periods T>3.5 seconds, we employed a two-pass elliptical filter (low-pass corner at ¼ Hz) identically on the data and the 3DSEM synthetic to permit direct comparison.

3.1 Models tested

Waveform studies of the upper inner core show little evidence for compressional wave discontinuities near 100 km depth in the propagation bands 0.1–3 Hz [17] and ~1 Hz [18–20]. At ~0.5 Hz, Cormier and Attanayake [21] have found a 1% V_P discontinuity 140 km below the ICB centered beneath the Atlantic Ocean—yet not evident elsewhere. We approached the study of the *PKIIKP* precursors from the perspective of the compressional velocity V_P, casting a wide net of ten possible V_P models to capture the features of the precursors—principally relative time and amplitude—with respect to *PKIKP* and *PKIIKP*. Models were limited to isotropic changes to inner core radial velocities in this paper. The series of models with a solid–liquid boundary at ~100 km depth met the timing of $PKI_{?}IKP$, but not the amplitude. Whereas most details of the inner core shear wave structure are unresolved, complexities such as 3D structures and anisotropy clearly are expressed in prior P-wave studies, e.g., [22–24]. We finally considered the effect of V_S on $PKI_{?}IKP$. Changing the value of V_S below a solid-liquid interface directly changed the amplitude of $PKI_{?}IKP$ without altering its travel time relative to *PKIKP* and *PKIIKP*.

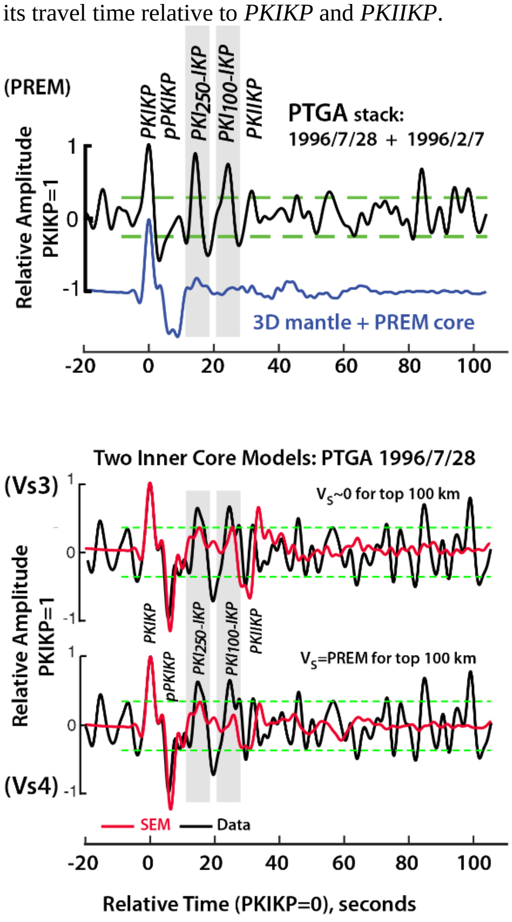

Figure 4. (upper) PTGA data (black) are stacked for two earthquakes on 1996/2/7 and 1996/7/28 in the upper trace—3DSEM synthetics (blue) are individually computed and stacked for PREM. The traces normalized to PKIKP. Although there are evident arrivals matching the timing of PKI100 IKP, PKI250-IKP, and PKIIKP in the stacked data, these phases are not evident in the PREM 3DSEM synthetic waveform (blue). (lower) Two traces compare PTGA data (black) from the 1996/7/28 event only, computed for two models which differ only above 100 depth, where VS = 0 (liquid) or VS = PREM (solid). Common model features include: (1) apparent discontinuities at 100 km and 250 km depth bounding an inner core region where shear velocity VS = 5 km/s; and (2) VS = PREM below 250 km depth. Two arrivals shaded in gray are clearly evident in the stacked data, and indicate the times of PKIIKP precursors from Figure 2. For PKI100 IKP observed 7 seconds before PKIIKP, the (upper) larger amplitude is consistent with a liquid/solid interface. Determined from modeling the same structure below 100 km depth, PKI250-IKP exhibits a self-consistent arrival for both models.

3.1.1 TAM and PTGA

Two earthquakes antipodal to TAM are modelled in Figure 3—a normal faulting event in 2011 and a thrust earthquake source from 1992. In these models V_P and density are unchanged from PREM values in the inner core, and V_S is modified in steps between 2.5–6.0 km/s. Decreasing V_S below that for PREM decreases the amplitude of $PKI_{?}IKP$, whereas increasing V_S effectively increased its amplitude. To attain the relative amplitudes observed for $PKI_{?}IKP/PKIKP$, we found that V_S must be ≥5 km/s. Having a candidate phase that has an appropriate amplitude and arrival time, we recognize that $PKI_{?}IKP$ has a standard seismic phase name of $PKI_{100}\text{-}IKP$ (Schweitzer, et al., 2019) as an underside reflection from an interface at z = 100 km deep below the ICB. The PTGA stacked observation of $PKI_{100}\text{-}IKP$ (Figure 2B) is most similar to TAM, both in the stacked amplitude and phase-weighted ratios (>50% of *PKIKP*), and relative timing. The PTGA stacked data corroborate the TAM observations (Figure 2). TAM and PTGA do not share common near-source, near-receiver, mantle, or outer-core propagation paths, and therefore the commonalities seen in the TAM and PTGA stacks then resides in shared inner core structure. However, this shared structure must thereby exist over two substantially different sections of the inner core. Given the corroboration of TAM and PTGA observations of $PKI_{??}IKP$, we have proceeded within the framework applied to $PKI_{100}\text{-}IKP$, but deeper within the central core. To model the observation of $PKI_{??}IKP$ at PTGA we synthesize two models (Figure 4) to test for a deeper, shear wave interface below $PKI_{100}\text{-}IKP$. Figure 4 shows that PTGA is not well fit by PREM. By timing considerations, an apparent discontinuity near a depth of 250 km (150 km thickness, with a $V_S \geq 5$ km/s) overlying PREM structure presents a reasonable fit to the PTGA data. In Figure 4, the two end-member models considered differ (liquid vs solid) only above z=100 km. We see $PKI_{250}\text{-}IKP$ in Figure 4 expressed nearly identically—e.g., the structure above 250 km does not contribute substantially to $PKI_{250}\text{-}IKP$. However, note that for a *P* wavelength of ~50 km, we cannot easily distinguish a sharp interface—whether at 100 or 250 km depth— from a narrow transition gradient. These models are not unique but do capture the essence of the data.

3.1.2 QIZ, ENH, and XAN

The antipodal stacks for QIZ, ENH, and XAN in China and PTGA in Brazil (Figure 2B) show the substantial diversity of the observations of $PKI_{100}\text{-}IKP$ for paths between South America and Southeast Asia (Figure 1). The PTGA stack differs significantly from those for QIZ, ENH, and XAN—

where there is no firm evidence of a *PKI*$_{100}$*-IKP* arrival in the stacked data in the Chinese station data. The neighboring Chinese stations—QIZ, ENH, XAN—fit the PREM model better, in marked contrast to TAM and PTGA.

4. Results and analysis

The *PKI*$_{100}$*-IKP* interface is not manifested in the same form everywhere. However, to match both TAM and ENH simultaneously, three-dimensional, uppermost inner-core structure must be considered. The TAM–Tonga annulus is nearly orthogonal to the annuli between Chile and the Chinese stations. Whereas the timing of *PKI*$_{100}$*-IKP* integrates over the propagation surface within the upper inner core, the amplitude constraint on *PKI*$_{100}$*-IKP* depends principally on the midpoint reflection, wherein the ray surface effectively coalesces to a great circle around the upper central core, orthogonal to the propagation direction midway between source and receiver.

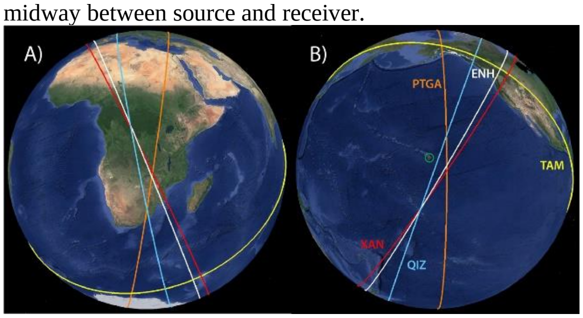

Figure 5. The great circles show the projection (AB) to the Earth's surface of the PKIIKP and PKI100 IKP midpoint reflection, great-circle arcs within the upper core. For scale at the ICB, the small green circle in (A) centered on Hawai'i Island has a projected diameter of 1 wavelength on the inner-outer core boundary. TAM (yellow) and PTGA (orange) both observe PKI100 IKP and PKI250-IKP, though propagating over substantially differing paths. For the neighboring paths of XAN, ENH, and QIZ (red, white, blue, respectively) within the upper central core, evidence for PKI100 IKP reflecting from a mushy liquid–solid interface at 100 km is absent, though a solid-solid interface cannot be rejected in every respect.

4.1 Reflection great circles

The location of the reflection great circle for TAM is shown in yellow in Figures 5 where *PKIIKP* reflects from the ICB and *PKI*$_{100}$*-IKP* reflects from the apparent discontinuity (V_S $\geq$ 5 km/s) at 100 km depth below the ICB. surface. TAM shows little overlap with the nearly orthogonal coverage by QIZ, ENH, and XAN, whose great circle paths differ by no more than six wavelengths between QIZ and XAN. For TAM the overlap with QIZ, ENH, and XAN is essentially two wavelengths, where their arcs cross over TAM's arc. For PTGA (orange) which shares the observations of *PKI*$_{100}$*-IKP* with TAM, its reflection great circle is within about $\Delta = 20°$ of the QIZ, ENH, and XAN neighborhood. The coverage of *PKI*$_{100}$*-IKP* by TAM and PTGA display very similar characteristics, although their propagation paths differ broadly. Hence, common inner core structures include not only proximal stations (QIZ, ENH, and XAN), but also broadly distinct propagation surfaces (TAM and PTGA). Comparing the narrow, great-circle reflection coverage of the QIZ, ENH, and XAN with the wider, great-circle reflection coverage of the TAM and PTGA suggests that the latter coverage of the inner core is more extensive than the former and therefore may be more representative of the inner core.

5. Summary

In this study of the inner core of Earth we have successfully employed the 3D Spectral Element Method on the Earth Simulator to model seismic structures within the upper inner core detected from antipodally amplified energy traversing the inner core. That two sets of data are presented—TAM (Algeria) and PTGA (Brazil) both show clear seismic arrivals, whereas the Chinese stations (XAN, ENH, QIZ) do not—indicates a significant shear wave velocity heterogeneity within the upper inner core. We have determined through synthetic modeling that two seismic precursors observed —PKI$_{100}$-IKP and PKI$_{250}$-IKP—are due to underside reflections from apparent discontinuities near 100 and 250 km beneath the ICB. In contrast to the Chinese stations which fit a PREM-like structure in the inner core, for PTGA and TAM the only inner core model found matching the seismic data constraints approximates a V_S solid-liquid discontinuity near 100 km depth where $V_S \geq 5$ for the solid. However, waveform data cannot resolve differences between liquid and "mushy" region. The PREM model has guided mineral physicists in their quest for understanding the low shear wave velocity within the inner core. Nonetheless, we now see body-wave reflection evidence for shear wave velocities ≥ 5 km/s from an upper core interface that comports with high shear wave velocity, iron-nickel alloyed compositions. Whereas we have antipodally interrogated the inner core with compressional body waves, our results are specifically derived from measured reflection amplitudes and times dependent upon shear wave velocity contrasts at apparent discontinuities 100–250 km beneath the traditional ICB. Where a discontinuity is not observed, the inner core structure more closely approximates PREM.

Acknowledgments and data availability

Data were obtained from GEOSCOPE and the IRIS Data Management System. We used the computer program (SPECFEM3D) for Spectral-Element Method. All the computations are performed using the Earth Simulator at the Earth Simulator Center of JAMSTEC. Centroid moment tensor solutions (GCMT) are used for synthetic models. We thank GEOSCOPE, USGS and NSF, and NCDSN China for the operation and maintenance of the seismic station used in this study. All data were downloaded from the IRIS Data Management System. Earthquake parametric data were downloaded from the USGS earthquake catalog. Earthquake source mechanisms were downloaded from the Global Centroid Moment Tensor database.

References

[1] Rial, J.A. and Cormier, V.F., 1980. Seismic waves at the epicenter's antipode. *Journal of Geophysical Research: Solid Earth*, *85*(B5), pp.2661-2668.
[2] Butler, R., 1986. Amplitudes at the antipode. *Bull. Seismol. Soc. Am.* 76, 1355–1365.
[3] Niu, F., and Chen, QF, 2008. Seismic evidence for distinct anisotropy in the innermost inner core. Nature Geosci., 1, 692–696 (2008). https://doi.org/10.1038/ngeo314
[4] Butler, R., and Tsuboi, S., 2010. Antipodal seismic observations of temporal and global variation at Earth's inner-outer core boundary. *Geophys. Res. Lett.* 37, L11301. https://doi.org/10.1029/2010GL042908https://doi.org/10.1029/2010GL042908.
[5] Cormier, V.F., 2015. Detection of inner core solidification from observations of antipodal PKIIKP. *Geophysical Research Letters*, *42*(18), pp.7459-7466.
[6] Attanayake, J., Thomas, C., Cormier, V. F., Miller, M. S., & Koper, K. D. (2018). Irregular transition layer beneath the Earth's inner core boundary from observations of antipodal PKIKP and PKIIKP waves. *Geochemistry, Geophysics, Geosystems*, *19*. https://doi.org/10.1029/ 2018GC007562
[7] Tsuboi, S. and R. Butler, 2020. Inner core differential rotation rate inferred from antipodal seismic observations. P*hysics of Earth and Planetary Interiors*, 301, April 2020, 106451, doi.org/10.1016/j.pepi.2020.106451.
[8] Butler, R. and Tsuboi, S., 2020. Antipodal observations of global differential times of diffracted P and PKPAB within the D″ layer above Earth's core–mantle boundary. Geophysical Journal International, 222(1), pp.327-337.
[9] Schimmel, M. and Paulssen, H., 1997. Noise reduction and detection of weak, coherent signals through phase-weighted stacks. *Geophysical Journal International*, *130*(2), pp.497-505
[10] Komatitsch, D. & Vilotte, J.P., 1998, The spectral-element method: an efficient tool to simulate the seismic response of 2D and 3D geological structures, *Bull. seism. Soc. Am.*, **88,** 368–392.
[11] Komatitsch, D., Ritsema, J. & Tromp, J., 2002. The spectral-element method, Beowulf computing, and global seismology, *Science*, **298,** 1737–1742 (2002).
[12] Tsuboi, S., D. Komatitsch, C. Ji, and J. Tromp, 2003. Broadband modeling of the 2002 Denali Fault earthquake on the Earth Simulator. *Phys. Earth Planet. Inter.* 139, 305–312.
[13] Komatitsch, D., Tsuboi, S. & Tromp, J., 2005. The spectral-element in seis- mology, in *Seismic Earth: Array analysis of broadband seismograms,*eds Levander, A. & Nolet, G., *AGU Geophysical Monograph* 157, 2005, AGU, pp. 205–227.
[14] Kustowski, B., Ekström, G. and Dziewoński, A.M., 2008. Anisotropic shear-wave velocity structure of the Earth's mantle: A global model. *Journal of Geophysical Research: Solid Earth*, *113*(B6).
[15] Bassin, C., G. Laske, and G. Masters, 2000. The current limits of resolution for surface wave tomography in North America, Eos Trans. AGU, 81, F897.
[16] Ekström, G., M. Nettles, and A. M. Dziewonski, 2012. The global CMT project 2004-2010: Centroid-moment tensors for 13,017 earthquakes, Phys. Earth Planet. Inter., 200-201, 1-9doi:10.1016/j.pepi.2012.04.002.
[17] Stroujkova, A., and V. F. Cormier, 2004. Regional variations in the upper-most 100 km of the Earth's inner core, J. Geophys. Res., 109, B10307, doi:10.1029/2004JB002976
[18] Leyton, F., Koper, K.D., Zhu, L. and Dombrovskaya, M., 2005. On the lack of seismic discontinuities within the inner core. *Geophysical Journal International*, *162*(3), pp.779-786.
[19] Yu, W.C. and Wen, L., 2006. Seismic velocity and attenuation structures in the top 400 km of the Earth's inner core along equatorial paths. *Journal of Geophysical Research: Solid Earth*, *111*(B7).
[20] Cormier, V.F., Attanayake, J. and He, K., 2011. Inner core freezing and melting: Constraints from seismic body waves. *Physics of the Earth and Planetary Interiors*, *188*(3-4), pp.163-172.
[21] Cormier, V.F. and Stroujkova, A., 2005. Waveform search for the innermost inner core. *Earth and Planetary Science Letters*, 236(1-2), pp.96-105.
[22] Tanaka, S. and Hamaguchi, H., 1997. Degree one heterogeneity and hemispherical variation of anisotropy in the inner core from PKP (BC)–PKP (DF) times. *Journal of Geophysical Research: Solid Earth*, *102*(B2), pp.2925-2938.
[23] Ishii, M., and A. M. Dziewonski, 2002. The innermost inner core of the Earth: Evidence for a change in anisotropic behavior at the radius of about 300 km, *Proc. Natl. Acad. Sci. U. S. A.*, **99**, 14,026–14,030, doi:10.1073/pnas.172508499.
[24] Waszek, L. and Deuss, A., 2011. Distinct layering in the hemispherical seismic velocity structure of Earth's upper inner core. Journal of Geophysical Research: Solid Earth, 116(B12).